Nucleation and first-stage growth processes of extrinsic defects in GaAs triggered by self-interstitials

F. Gala* and G. Zollo

Dipartimento di Energetica, Universitá di Roma "La Sapienza" and Consorzio Nazionale Interuniversitario per le Scienze Fisiche della Materia (CNISM), Via A. Scarpa 14-16, 00161 Rome, Italy

(Received 7 August 2009; published 19 November 2009)

The growth process of small self-interstitial clusters I_n ($n \leq 7$) in crystalline GaAs has been addressed by semi-empirical tight-binding molecular-dynamics technique. The I_n ground-state structures have been found among many possible choices of topological properties and stoichiometric compositions. The stable structure have been fully characterised concerning the structural, electronic, energetic, and elastic properties; some remarkable findings emerged concerning, among the others, the stability scenario of the ground-state structures, the possible low-energy reaction paths involved in the growth process, the electrostatic and the elastic capture volumes and the Fermi-level pinning. It is demonstrated that compact geometries are no longer energetically favoured for $n \geq 5$ and that the I_n growth proceeds via capture processes involving either isolated interstitials or di-interstitials. An extended pentainterstitial (I_5) ground-state structure has been identified as the possible core-basic structure of extrinsic linear defects along the {111} direction of the GaAs lattice.

DOI: 10.1103/PhysRevB.80.174113 PACS number(s): 61.72.jj, 31.15.bu, 71.55.Eq

I. INTRODUCTION

In recent years a novel interest has been focussed onto the aggregation mechanisms of large crystal imperfections that may affect the properties of materials widely used in nanotechnology and electronics; gallium arsenide, thanks to its peculiar optoelectronic properties, is one of the most employed semiconductors for high-performance devices such as terahertz-wave generator[1,2] and for heterostructured transistors obtained with ion-implantation[3] or standard growth techniques. Previous works have shown that small point defects, such as antisites and vacancies are energetically favoured at thermodynamic equilibrium; far from the equilibrium also self-interstitial atoms with large formation energy must be considered and extrinsic extended defects with complex structures can be formed, as evidenced using lattice imaging techniques such as high-resolution transmission-electron microscopy.[4,5] This is the case, for example, of low-temperature-grown gallium arsenide (arsenic excess during deposition) or ion-implanted materials where a kick-out mechanism, triggered on by colliding ions, produces interstitials atoms migrating through the entire crystal and forming large structures up to nanometric scale. These imperfections usually interact with free carriers acting as traps or scattering centers and affecting the semiconductor properties and the devices performance.

The need of theoretical studies of such complexes is also due to the lack of experimental data concerning their atomic structure as a consequence of the resolution limits inherent all the microscopy techniques; therefore a certain number of studies on interstitial defects in GaAs can be found in the recent literature.[6–10] Fully quantum-mechanical computations, based on density-functional theory (DFT), and semi-empirical methods based on tight-binding molecular dynamics (TBMD) agree that the stable monointerstitial configurations (I_1) of Ga and As species are, respectively, the tetrahedral position and the ⟨110⟩ As-As dumbell.[11,12] Moreover these defects have been shown to exhibit, in general, an inverse anion-cation charge transfer with respect to the bulk semiconductor, and introduce several one-electron levels in the GaAs band gap as traps for charge carriers.

For what concerns the stable structure geometries involving I_2 point defects, semi-empirical molecular-dynamics calculations are in good agreement with *ab initio* total-energy methods showing that triangular complexes are energetically favoured. However some differences emerged for the stability hierarchy: from semi-empirical calculations the As_1Ga_1 interstitial has the lowest formation energy among the possible di-interstitial stochiometries[12] while DFT calculations predict the As_2 triangular structure as the most stable.[9,11]

As the complex size increases, *ab initio* calculations become computationally too heavy, making the tight-binding approach, validated for I_{1-2} complexes, as the most appropriate. For the I_3 complexes in GaAs, tight-binding calculations have shown that quasistochiometric clusters (those with almost the same number of Ga and As, namely, $As_xGa_{(3-x)}$ with $x=1,2$) exhibit lower binding energies (i.e., higher absolute values) among all the possible configurations.[13] Moreover, tetrahedral structures, formed by four atoms of which three are interstitials and one from the host crystal, located at the vertices of a tetrahedron whose center is the lattice site formerly occupied by the lattice atom, show the lowest binding energies. This can be explained in terms of elastic deformation induced by the interstitial defects into the host crystal lattice.

In this paper TBMD is used to study neutral I_n complexes in crystalline GaAs with $n \leq 7$. Sec. II is devoted to the computational method used in the present work and to the theoretical aspects concerning the stability, energetic, electronic, and elastic properties of the studied configurations. In Sec. III the criteria to select initial configurations are discussed and the results for the defect cluster geometries are reported together with the energetic, electronic, and elastic properties. In this section, moreover, the obtained results are deeply and critically discussed. Finally, in Sec. IV conclusions are outlined concerning the obtained results with a particular em-

 ©2009 The American Physical Society

phasis on the capture and aggregation processes of self-interstitials.

II. COMPUTATIONAL METHODS

In the semi-empirical TBMD, the total energy of the system is made of two terms: the first one is an attractive term accounting for electron-ion and (doubly counted) electron-electron interactions of the system; it is referred as the band-structure energy and it is computed by summing over the occupied states the eigenvalues of the single-particle hamiltonian matrix. The second one is a repulsive term, fitted analytically, containing the ion-ion interactions, the charge-transfer effects and the correction of the double counting in band-structure energy.[6,14]

The adopted parameterization,[15] developed for liquid and amorphous GaAs, is based on a linear combination of atomic orbitals made of sp^3s^* basis set for the single-particle electron wave function and only nearest-neighbour interactions are considered; the model has been successfully tested and is well suited for the study of point defects in crystalline GaAs.[12,13,16]

The energy minimization of the system is obtained via a molecular-dynamics-simulated annealing technique[17] (up to a target temperature of 300 K) and a subsequent damped dynamics to achieve the minimum of the metastable configuration that basically consists in introducing a fictitious friction coefficient to avoid energy fluctuations close to the local minima. Since the potential-energy surface becomes more and more complex as the number n of interstitial atoms increases, damped dynamics is essential to compare metastable structures having similar energies.

Simulations involving I_n interstitial have been performed in a tetragonal 640 atom supercell with periodic boundary conditions, reducing in this way spurious effects due to fictious interactions between the replicas of the simulation cell that may arise as a consequence of the increasing length of the structures studied.

Several energetic quantities are used to study the different configurations: the binding energy E_b, the second-order difference in total energy $\Delta_2 E$, and the relative formation energy Ω_{rel}.

The binding energy of an I_n interstitial cluster is defined as follows:[18]

$$E_b[I_n] = \Omega[I_n] - (n_i^{\mathrm{Ga}}\Omega[I_{\mathrm{Ga}_i}] + n_i^{\mathrm{As}}\Omega[I_{\mathrm{As}_i}]), \tag{1}$$

where $\Omega[I_n]$ is the formation energy of the complex, $\Omega[I_{\mathrm{Ga}_i}](\Omega[I_{\mathrm{As}_i}])$ is the formation energy of the Ga (As) isolated interstitial and $n_i^{\mathrm{Ga}}(n_i^{\mathrm{As}})$ are the number of Ga (As) interstitial atoms involved in the cluster. The formation-energy calculation requires the computation of the Ga and As chemical potentials in their stable bulk phases; unfortunately these quantities can not be computed in the frame of the present TBMD parametrization for GaAs and thus an algebraic method which avoids the computation of chemical potentials of the single species has been developed[12] and employed in the present work. If the components are labelled as x and y (x=Ga/As), the binding energy of I_n (with $n=n_i^x+n_i^y$) results to be

$$E_b[I_n] = \begin{cases} E_D[I_n] - n_i(E_D[I_{\mathrm{Ga}_i}] + E_D[I_{\mathrm{As}_i}]) + \frac{1}{2}\mu_{\mathrm{GaAs}}\mathcal{N}[2n_i - 1], & n_i^x = n_i^y = n_i \\ E_D[I_n] - (n_i^x E_D[I_{x_i}] + n_i^y E_D[I_{y_i}]) - \frac{1}{2}\mu_{\mathrm{GaAs}}[3n_i^y + \mathcal{N}(1 + 2n_i^y - n_i^x)], & n_i^x > n_i^y \end{cases}, \tag{2}$$

where the first expression is for "stochiometric clusters" (i.e., clusters with the same number of Ga and As interstistials) and the second for "nonstochiometric clusters" ($n^{\mathrm{Ga}_i} \neq n^{\mathrm{As}_i}$).

$E_D[I_n]$, $E_D[I_{\mathrm{Ga}_i}]$, and $E_D[I_{\mathrm{As}_i}]$ are the total energies of the supecells containing, respectively, the interstitial cluster, the isolated Ga interstistial and the isolated As interstitial, μ_{GaAs} is the bulk GaAs chemical potential and $\mathcal{N}$ is the atom number of the bulk supercell. The binding energy defined in Eq. (1), that can be roughly considered as the energy needed to split the cluster into single point defects, is a measure of the energy gain of the structure with respect to the stable configuration containing the same number of isolated interstitials.

However $E_b[I_n]$ gives no information about the stability of the I_n complex with respect to its "neighbours" I_{n+1} and I_{n-1}. Following a common practice in the field of cluster physics[19] the second energy difference $\Delta_2 E$ is used at this purpose and can be obtained by varying the size of the complex as

$$\Delta_2 E[I_n] = E_D[I_{n+1}] - 2E_D[I_n] + E_D[I_{n-1}]. \tag{3}$$

From the above expression it is clear that those clusters having positive values of $\Delta_2 E$ are more stable with respect to its nearest neighbours because $\Delta_2 E$ is nothing but the difference between the energies of the reactions $I_{n-1}+I_1 \rightleftharpoons I_n$ and $I_n+I_1 \rightleftharpoons I_{n+1}$ (see below) if the added monointerstitial belongs to the same species for both the reactions. If the monointerstitials involved in the two reactions are chemically different, the difference in the reaction energies must be shifted by $\pm[E_D(\mathrm{As}_1)-E_D(\mathrm{Ga}_1)]$.

Finally, the relative reaction energy of the process $I_{n-m}+I_m \rightleftharpoons I_n$ has been computed with the help of the same algebraic method adopted for computing the binding energies in Eq. (2)

$$\Omega_{rel}^{(m)}[I_n] = E_D[I_n] - (E_D[I_{n-m}] + E_D[I_m]) + \frac{1}{2}\mathcal{N}\mu_{\mathrm{GaAs}},$$

$$1 \le m \le \left[\frac{n}{2}\right], \tag{4}$$

where $[x]$ is the integer part of x.

The reaction is endothermic (exothermic) if $\Omega_{rel}^{(m)} > 0$ ($\Omega_{rel}^{(m)} < 0$). Exothermic reactions favor the formation of larger clusters to the detriment of the two smaller reactants. Moreover it should be noted that, in the special case $n=2$ and $m=1$, the relative reaction energy is equal to the binding energy of the cluster.

The electronic properties of the complexes have been analyzed in terms of standard tools such as Mulliken population analysis for charge transfer between atoms, the electron density of states, the one-electron wave-function localization properties, and the highest occupied molecular orbital-lowest unoccupied molecular orbital (HOMO-LUMO) gap.

Since previous works[13] have shown that local lattice strain field on the atoms of the host crystal plays a central role in understanding the stability and geometrical properties of a self-interstitial cluster in GaAs, the capture volume for a mobile diffusing species has been computed through the defect-induced strain field. A local strain field can be defined by comparing the relative atomic positions of the final strained configuration to those ones of a theoretical final configuration obtained in the case of a uniform local strain field $\epsilon_{\mu\nu}$ (affine deformation). This is implemented by defining the following quantity:

$$D^2(\mathbf{X}^k, \overline{\mathbf{X}}^k) = \sum_{n \in \Omega_k} \sum_{\mu} \left[\Delta X_\mu^{nk} - \sum_{\nu} (\delta_{\mu\nu} + \epsilon_{\mu\nu}(\mathbf{X}^k, \overline{\mathbf{X}}^k)) \Delta \bar{X}_\nu^{nk} \right]^2, \tag{5}$$

where the indices μ and ν indicate spatial coordinates, n and k run over the particles of the system, Ω_k is the set of the nearest neighbours of the kth atom, $\mathbf{X}^k$ and $\overline{\mathbf{X}}^k$ are the position of the kth atom in the strained and in the reference configurations, respectively, and $\Delta\mathbf{X}^{nk} = \mathbf{X}^n - \mathbf{X}^k$.

The local strain tensor $\epsilon_{\mu\nu}$ can be evaluated by minimizing D^2 that is nothing but the local deviation from an affine deformation connecting the reference and the strained configurations.[20] The minimum value of D^2 is obtained by evaluating the auxiliary matrices $\hat{A}^{(k)}$ and $\hat{B}^{(k)}$

$$A_{\alpha\beta}^{(k)} = \sum_n \Delta X_\alpha^{nk} \Delta \bar{X}_\beta^{nk},$$

$$B_{\alpha\beta}^{(k)} = \sum_n \Delta \bar{X}_\alpha^{nk} \Delta \bar{X}_\beta^{nk}$$

from which the local strain tensor on the kth atom results to be

$$\epsilon_{\mu\nu}(\mathbf{X}^k, \overline{\mathbf{X}}^k) \equiv \epsilon_{\mu\nu}^{(k)} = \sum_\sigma A_{\mu\sigma}^{(k)} B_{\nu\sigma}^{(k)-1} - \delta_{\mu\nu}. \tag{6}$$

Strained volumes have been computed through the relation $\Delta V^{(k)}/V_0^{(k)} \simeq \mathrm{Tr}[\epsilon^{(k)}]$ that measures of the effects of the strain deformations on a small volume element $V_0^{(k)} = l_{0x} l_{0y} l_{0z}/\mathcal{N}$ containing the kth atom of the crystal lattice in a bulk supercell that has edge lengths of l_{0x}, l_{0y}, l_{0z} and includes $\mathcal{N}$ atoms. Thus the total capture volume of the inclusion has been evaluated as the volume of the region containing the strained atoms, i.e., those ones with $\Delta V^{(k)}$ values greater than a given treshold.

In the frame of the present approach the relative relaxation volume can be easily calculated by summing the local deformations, i.e., by summing the traces of the local strain tensors, over the atomic sites of the deformed lattice. The same quantity is commonly calculated in the literature via the following relation:

$$\frac{\Delta V^{rel}}{V_0} = \left(\frac{l_x}{l_{0x}}\right)\left(\frac{l_y}{l_{0y}}\right)\left(\frac{l_z}{l_{0z}}\right) - 1 \tag{7}$$

that requires the total energy minimization by varying the supercell lattice constant in order to find the equilibrium volume of the supercell containing the inclusion.[21] Our approach, however, has the main huge advantage to allow the evaluation of the local strain and, consequently, the drawing of strain field maps that could evidence the existence of possible preferential diffusion paths close to the inclusions.

III. RESULTS AND DISCUSSION

In a binary semiconductor, such as gallium arsenide, the allowed stochiometries for a self-interstial cluster I_n are $n+1$. Moreover the topology of I_n with a specific stoichiometric composition could be chosen among many possible configurations. Since the task of studying all the possible stoichiometries and topology of all I_n is unattainable, it has been decided to restrict the analysis to a class of configurations chosen on the basis of the previous results on I_3. Previous works[12,13] have shown that stoichiometric clusters are energetically favoured and thus in the following only aggregates with (almost) the same number of Ga and As will be considered. Even though a comprehensive discussion on the main properties of I_1, I_2, and I_3 stable configurations can be found in the cited papers, some of them are summarized in Fig. 1 for convenience.

All the starting configurations investigated in the present work are those obtained via the kinematical reaction $I_{n-m} + I_m \rightleftharpoons I_n$ with $1 \le m \le [\frac{n}{2}]$. For $m=1$ the process of aggregation of a single monointerstitial to an extended structure is considered through the reaction $I_n + I_1 \rightleftharpoons I_{n+1}$, to form stoichiometric (or quasistoichiometric) clusters. For the $m>1$ case, the aggregation and coalescence of two interacting complexes is studied. One example of the coalescence process between two complexes containing more than one interstitial is shown in Fig. 4(b), where an I_3 tetrahedron interacts with a triangular I_2 structure to form an extended I_5 complex.

A. Structural properties

Examples of starting configurations for As_2Ga_2 complexes are summarized in Fig. 2; white circles in Fig. 2(a)

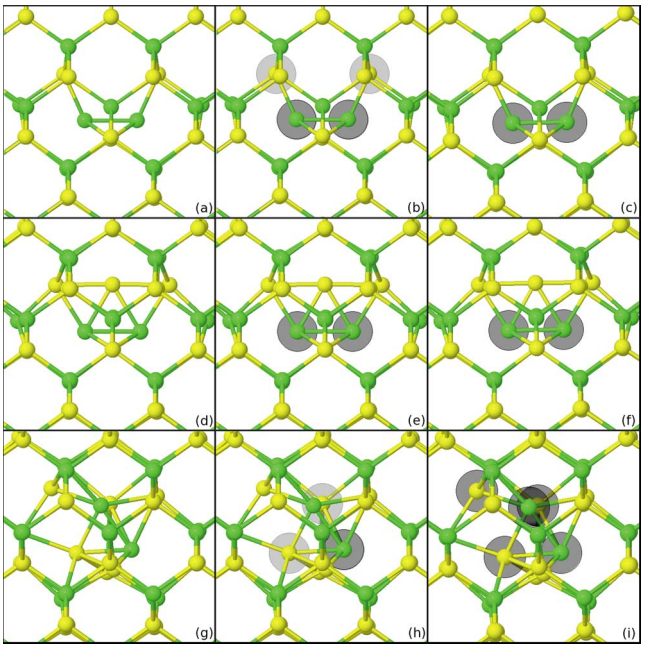

FIG. 1. (Color online) (110) Plane view of (a) I_1, (d) I_2, and (g) I_3 stable configurations. As and Ga atoms are in dark gray (green online) and light gray (yellow online), respectively. Correspondingly the total charge transfer with respect the bulk phase are shown in (b), (e), and (f) for I_1, I_2, and I_3 with positive and negative charge transfer in gray and black halos, respectively; localization map of the one-electron wave function of the occupied levels in the band gap of bulk GaAs is evidenced with black halos in (c), (f), and (i) for I_1, I_2, and I_3.

indicate the closest tetrahedral interstitial sites that have been considered for the reaction $I_3+I_1 \rightleftharpoons I_4$ involving an As interstitial and the most stable I_3 complex, namely, the As_1Ga_2 tetrahedron.[13] Figure 2(b) shows an example of two interacting di-interstitials, one of them being the most stable As_1Ga_1

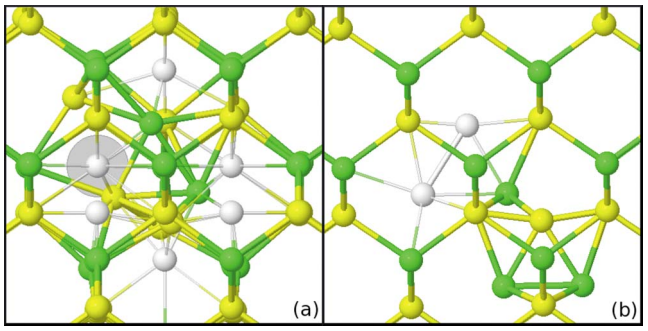

FIG. 2. (Color online) Starting configurations for As_2Ga_2 interstials in crystalline GaAs (see the caption of Fig. 1 for the color code employed); the structure (a) is obtained from the most stable As_1Ga_2 tetrahedral configuration, resulting from previous investigations (Ref. 13) and an extra As atom placed in one of the possible closest tetrahedral sites (white positions, gray halo is for the most stable one after optimization) while (b) reports one possible example of the interaction of extended clusters via the reaction $As_1Ga_1+I_2 \rightleftharpoons As_2Ga_2$, obtained from the stable triangular complex As_1Ga_1 as in Ref. 12 and two interstitials forming a triangle on a crystal site.

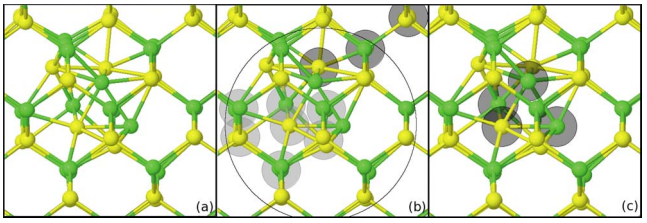

FIG. 3. (Color online) (a) Energetically stable configuration in the (110) plane for the As_2Ga_2 complex (see the caption of Fig. 1 for the color code employed). In (b) it is reported that the charge transfer map with respect to the bulk phase, (positive/negative charge transfer corresponds to gray/black halos). It is also evidenced the sphere corresponding to the charge maximum of Fig. 12. In (c) the localization map of the one-electron wave function of the occupied levels in the band gap of bulk GaAs (black halos) is reported.

structure[12] while the other is a triangular structure (with stoichiometry As_1Ga_1) on a neighboring crystal site.

There are ten possible tetrahedral sites where an extra atom can be added nearby the As_1Ga_2 complex: eight lateral with different environments and two vertical sites; these sites are marked as white atoms in Fig. 2(a) where some of them are hidden by other superimposed tetrahedral sites. After performing the optimization tools described in Sec. II, namely, a simulated annealing run followed by a damped dynamics at 0 K, it comes out that only the last two configurations result in metastable structures in which the original tetrahedron is almost unchanged. On the contrary the other starting configurations result, upon optimization, in the splitting of the original tetrahedron into two triangles as the ones visible in the most stable I_4 configuration of Fig. 3(a). The triangles of this complex are of mixed stoichometry on different crystal sites: one on an As site with side lengths of approximately 2.69, 2.58, and 2.53 Å, the other on a Ga site with side lengths of 2.75, 2.66, and 2.46 Å. The same stable geometry can be obtained also through the reaction $I_2+I_2 \rightleftharpoons I_4$ with a starting configuration similar to the one reported in Fig. 2(b).

It is worth to emphasize that the relaxed geometry is no longer a compact structure around a single lattice site but, on the contrary, start to be extended involving two lattice atoms and plastically deforming the host crystal locally to form triangular structures on different adjacent lattice sites. In the whole the obtained structure shows some tendency to organize itself in a "faceted" structure even though this circumstance will emerge more clearly for larger clusters. This means that $n=3$ is the largest cluster size allowing the formation of a stable compact cluster geometry around a single site.

For I_5 complexes, two different reaction paths have been studied: the first one, as for the previous case, is obtained by adding a single monointerstitial atom of either Ga or As species to the most stable As_2Ga_2 configuration in the closest tetrahedral positions. These positions are twelve, eight with a lateral self-interstitial, two with a vertical inclusion, and two in the middle, and the corresponding starting geometries are reported in Fig. 4(a). The second process studied is the coalescence of I_2 and I_3, namely, the reaction $I_3+I_2 \rightleftharpoons I_5$ that involves the stable As_1Ga_2 tetrahedral configuration interact-

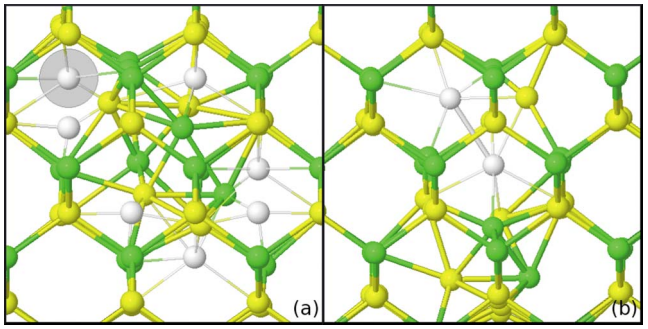

FIG. 4. (Color online) Starting configurations for I_5 interstitials (see the caption of Fig. 1 for the color code employed). Configurations in (a) are obtained from the most stable As_2Ga_2 reported in Fig. 3 and an extra interstitial atom placed in one of the possible closest tetrahedral sites (white positions, the one with a grey halo originates, after optimization, the most stable configuration among that studied in the present work). In (b) it is drawn one of the possible examples of the interaction of a tetrahedron complex with a triangular complex, obtained from the stable As_1Ga_2 complex and a dimer forming a triangle on an adjacent crystal site.

ing with a stable I_2 triangular structure. The last one has been selected due to its stability properties as follows from previous investigations[12,13] while the stoichiometries of the reactant I_2 complexes are either As_1Ga_1 or As_2, chosen in order to obtain quasistoichiometric clusters. An example of such starting configuration is reported in Fig. 4(b). The optimization of these initial configurations has shown that all of them are at least metastable structures even if those involving extended reactants are in general less stable than those obtained via single-atom defect aggregation. The most stable I_5 configuration turned out to be the one reported in Fig. 5(a) with a stoichiometry of As_3Ga_2. It has been obtained via a kick-out process where the added As interstitial kicks out from its site the upper left Ga atom forming two triangles with the same stoichiometry: a base formed by a Ga_1As_1 dimer and a vertex occupied by an As interstitial. Both triangles are approximately isosceles: the one at the Ga site has 2.7, 2.59, and 2.5 Å side lengths; the other, at the As site, has 2.70, 2.58, and 2.52 Å side lengths. The kicked-out Ga interstitial stays nearby in a local energy minimum to form another triangular structure showing no particular symmetry (2.74, 2.70, and 2.48 Å side lengths) and lying out of the (110) plane of the figure. The stable structure found starts to be

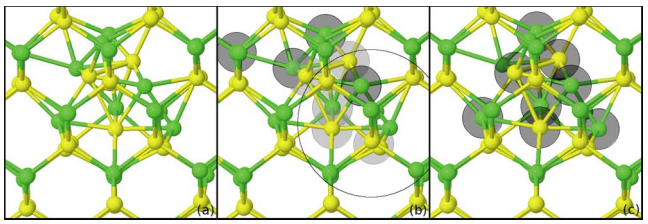

FIG. 5. (Color online) Energetically stable configuration in the (110) plane for the As_3Ga_2 complex, total charge transfer with respect to the bulk phase and localization map of the one-electron wave function are reported, respectively, in (a), (b), and (c). See the caption of Fig. 3 for details on the color code employed.

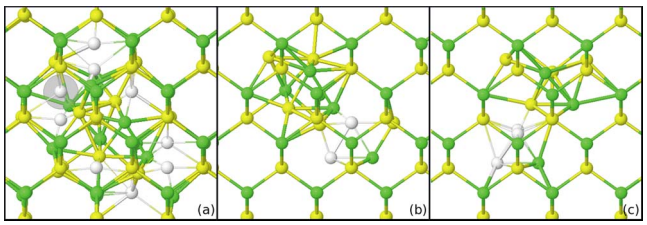

FIG. 6. (Color online) Starting configurations for I_6 interstials (see the caption of Fig. 1 for the color code employed). Configurations in (a) are obtained from the most stable As_3Ga_2 reported in Fig. 5 and an extra interstitial atom placed in one of the possible closest tetrahedral sites (white positions and, as the previous cases, the gray halo identifies the one resulting in the stable configuration after optimization). In (b) it is shown one of the possible examples of the interaction of a stable I_4 self-interstitial with a triangular complex. Finally in (c) it is reported as an example of starting configuration obtained with the interaction of two tetrahedrons.

extended along the $[1\bar{1}1]$ direction of the crystal lattice [in the (110) plane of the figure] shows a clear faceted structure that lies in the (110) and $(10\bar{1})$ planes of the GaAs crystal structure.

Owing to the reasons explained above, only stoichiometric clusters As_3Ga_3 have been considered for I_6 complexes. The starting geometries are summarized in Fig. 6 and, as in the previous cases, configurations in Fig. 6(a) are obtained from the stable As_3Ga_2 interstitial cluster by adding one Ga atom in one of the thirteen nearest tetrahedral sites (white positions). Both Figs. 6(b) and 6(c) are examples of reaction paths involving structured complexes. In the first one an As_2Ga_2 interstitial cluster interacts with a stable As_1Ga_1 complex while in the second one an As_2Ga_1 inclusion interacts with a tetrahedron (I_3) characterized by two possible stoichiometries: As_1Ga_2 and As_2Ga_1.

After the optimization tool, it comes out that the most stable As_3Ga_3 configuration is made of the previously described stable As_3Ga_2 interstitial cluster and one Ga atom forming a rotated triangle with the atoms of the host crystal [Fig. 7(a)]. The inclusion of an extra Ga atom, which forms a scalene triangle with side lengths equal to 2.32, 2.52, and 2.77 Å, has modified slightly the I_5 structure, making the three triangles (see above) approximately isosceles. Distances are equal to 2.43, 2.75, and 2.8 Å for the one at the As site, 2.53, 2.65, and 2.69 Å for the one at the Ga site and for the triangle out of the (110) plane 2.53, 2.74, and 2.75 Å.

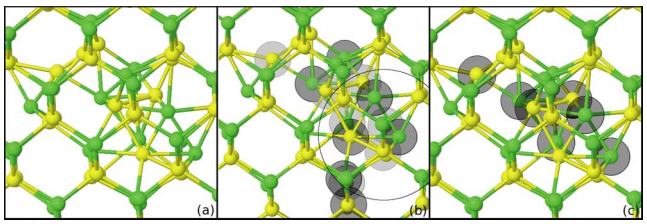

FIG. 7. (Color online) Energetically stable configuration in the (110) plane for the As_3Ga_3 complex, total charge transfer with respect the bulk phase and localization map of the one-electron wave function are reported, respectively, in (a), (b), and (c). See the caption of Fig. 3 for clarifications on the color code employed.

TABLE I. Energetic properties of I_n complexes with $1 \leq n \leq 7$; the binding energy E_b, the second-order difference in total energy $\Delta^2 E$, and the HOMO-LUMO gap are reported for stable I_n configurations, see Secs. II and III B for more details.

Defect	E_b (eV)	$\Delta_2 E$ (eV)	HOMO-LUMO (eV)	Levels in the band gap
As_1			0.61	1
As_1Ga_1	−3.18	1.69	0.80	1
As_1Ga_2	−4.65	−15.37	0.08	3
As_2Ga_2	−6.95	−0.07	0.43	4
As_3Ga_2	−9.31	15.88	0.50	4
As_3Ga_3	−10.36	−0.93	0.32	4
As_3Ga_4	−12.34		0.36	4

The same stable configuration results also from the reaction involving only I_3, namely, the $As_1Ga_2 + As_2Ga_1 \rightleftharpoons As_3Ga_3$. This reaction path shows the highest formation energy among the possible channels studied, as reported in Table II; after optimization, the As_2Ga_1 tetrahedron split into a distorted triangular complex involving one Ga and one As crystal atoms, and located far (~9 Å) from the As_1Ga_2 structure, plus an As_2 dimer that interacts tightly with the Ga atoms of the core tetrahedron.

The stable I_6 configuration extends along the $[1\bar{1}1]$ direction in the (110) plane of the figure and is made of triangular structures forming large facets lying in the (110) and $(10\bar{1})$ planes. Finally Fig. 8 shows the initial configurations studied for I_7 complex where, similarly to the previous cases, the different reaction paths are evidenced. In Fig. 8(a) white positions indicate the closest tetrahedral sites for a single interstitial interacting with the stable As_3Ga_3 complex previously described. In Figs. 8(b) and 8(c), instead, two examples of reaction paths are shown: the first one involves the stable As_3Ga_2 interacting with a stable I_2 complex either with stoichiometry As_1Ga_1 or Ga_2; in the second one, instead, the stable As_2Ga_2 can react with either As_1Ga_2 or As_2Ga_1.

After the optimization, the most stable configuration results to be an As_3Ga_4 complex illustrated in Figs. 9(a) and 9(d), showing the relaxed cluster geometry along the (110) and $(1\bar{1}0)$ planes, respectively. The extra Ga interstitial atom, added to I_6 to form a dumbbell, moves spontaneously in the

TABLE II. Relative formation energies of stable I_n configurations evaluated via Eq. (4). A detailed discussion on the interpretation of such results is presented in Sec. III B.

Defect	$\Omega_{rel}^{(1)}$ (eV)	$\Omega_{rel}^{(2)}$ (eV)	$\Omega_{rel}^{(3)}$ (eV)
As_1Ga_1	−3.18		
As_1Ga_2	−1.48		
As_2Ga_2	−2.29	−0.60	
As_3Ga_2	−2.37	−2.16	
As_3Ga_3	−1.05	−0.24	−2.15
As_3Ga_4	−1.98	−1.16	−0.74

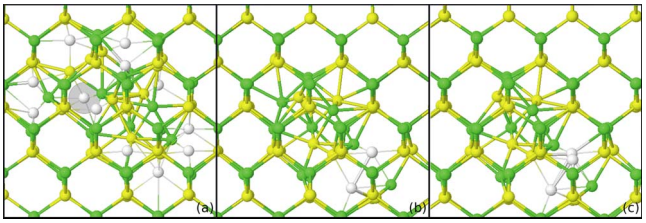

FIG. 8. (Color online) Starting configurations for I_7 interstials (see the caption of Fig. 1 for the color code employed). Configurations in (a) are obtained from the most stable As_3Ga_3 in Fig. 7 and an extra interstitial atom placed in all possible closest tetrahedral sites (white positions). In (b) one of the possible examples of the interaction of a stable I_5 self-interstitial with a triangular complex is reported. In (c) it is shown as an example of the starting configuration employed for the reaction $I_5 + I_2 \rightleftharpoons I_7$. After optimization the interstitial atom with a gray halo in (a) resulted to be the most stable among all the configurations investigated.

$(10\bar{1})$ plane, forming (approximately) an isosceles triangle at a Ga site with side lengths equal to 2.5, 2.56, and 2.79 Å. On the contrary the core of the stable As_3Ga_3 changes very little with a maximum deviance in side lengths of less than 6%. Still the growth process proceeds along the $[1\bar{1}1]$ direction of the (110) plane and the faceted structure becomes more and more pronounced.

B. Energetic properties

The stability of the investigated complexes, as mentioned before, can be discussed in terms of several energetic observables whose values, for the structures involved in the present work, are reported in Tables I and II, and in Fig. 10. The large binding values obtained for the stable configurations show that I_n complexes are, up to $n=7$, definitely favoured against the isolated interstitials indicating that wherever a source of interstitials is present, as, for instance, in implanted

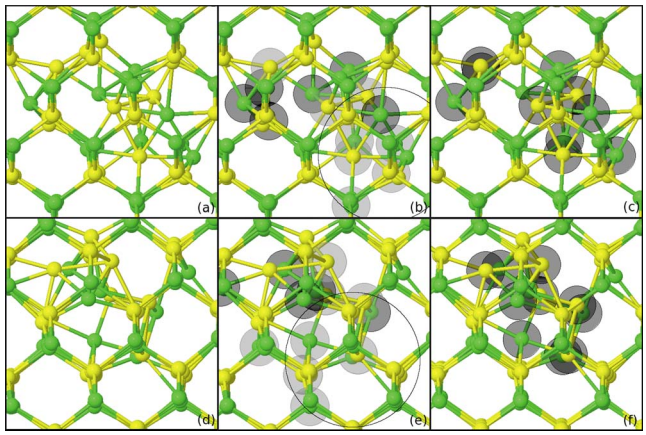

FIG. 9. (Color online) Energetically stable configuration in the (110) plane for the As_3Ga_4 complex, total charge transfer with respect to the bulk phase and localization map of the one-electron wave function are reported, respectively, in (a), (b), and (c); the same configuration, charge-transfer and localization maps are shown also in the $(1\bar{1}0)$ plane in (d), (e), and (f), respectively. See the caption of Fig. 3 for clarifications on the color code employed.

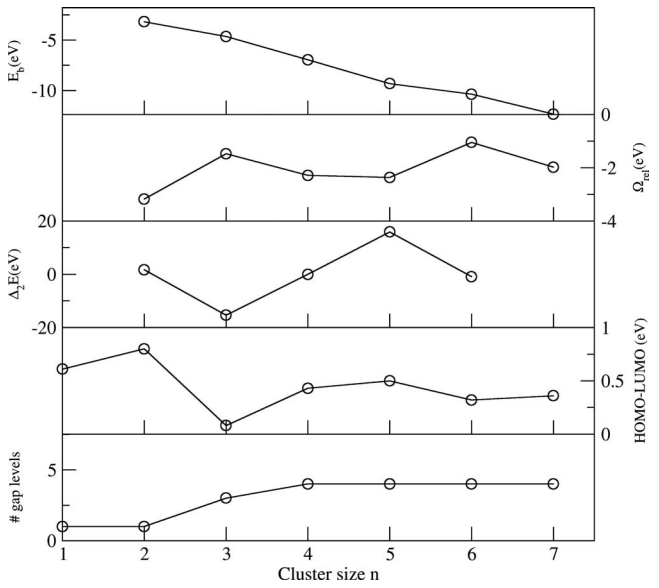

FIG. 10. From top to bottom: (a) binding energy of small compact interstitial clusters, (b) relative formation energy of the reaction $I_{n-1}+I_1 \rightleftharpoons I_n$, (c) second energy difference, (d) HOMO-LUMO gap, (e) and number of levels in the band gap of the GaAs bulk phase.

or low-temperature-grown GaAs, in principle we must expect the formation of I_n complexes.

Calculations show that the binding energies are large and decrease almost linearly with the increasing cluster: the calculated average binding-energy per interstitial [the average decreasing rate of the curve in Fig. 10(a)] is about 1.7 eV per added interstitial ranging from 1.55 eV for As_1Ga_2 to 1.86 eV for As_3Ga_2. These ground-state data show that, up to $n=7$, there is no sign of saturation in the curve of Fig. 10(a) indicating that we are far from the growth limit of such complexes; thus it is likely that such a behavior could be extrapolated to larger values of n, strongly supporting the hypothesis of interstitial mediated extended defects nucleation and growth in, for example, irradiated GaAs. However, the above reported ground-state data can not be considered conclusive as the existence of low-energy reaction paths, leading to interstitial capture by stable I_n complexes or to interstitial complexes coalescence into larger structures, must be checked to guarantee that the growth process really proceeds. This task would be completely fulfilled if the reaction activation energy were calculated; however, due to the complexity of the energy landscape involved in the present case (also related to the compound nature of GaAs), it is practically unattainable and thus we restricted the reaction path analysis to the study of the possible reactions and to the ground-state calculation of the related reaction energy. For these reasons many different reaction paths involving single interstitials and small complexes have been investigated and checked to this aim mainly by calculating the reaction energy through the Eq. (4). The reaction energy data are summarized in Table II and show that, for each stable I_n complex, low-energy reaction paths exist with large absolute values of $\Omega_{rel}^{(1)}$. Moreover the same data evidence that each stable structure can be obtained also via exothermic reactions involving structured reactants such as the reaction $I_3+I_3 \rightleftharpoons I_6$. Therefore some of the I_n stable structures can be obtained either via self-interstitial capture or through the coalescence of I_m and I_{n-m} $(m \leq n)$. The data in Table II show that, for all the I_n complexes but As_3Ga_3, the single interstitial capture reaction seems favoured against the possible reactions investigated; consider, for instance, the two different processes leading to the same final I_4 stable configuration, namely, the capture process of a single interstitial by a stable I_3 compact cluster and the coalescence reaction $I_2+I_2 \rightleftharpoons I_4$; the reaction energy data show that the last one has roughly a quarter of the activation energy of the process involving an I_3 and a single monointerstitial atom. As briefly mentioned, this general trend is violated in the case of the most stable I_6 configuration: in this case, indeed, the reaction involving two I_3 clusters is definitely more exothermic than the single monointerstitial capture process that is in striking contradiction with the other cases for which the single interstitial capture process seems the main mechanism for the formation of small and geometrically compact clusters. This behavior of I_6 is probably related to the high-stability properties of the As_3Ga_2 cluster testified by the large values of the reaction energy leading to this configuration, that disadvantages the reaction $As_3Ga_2+Ga_1 \rightleftharpoons As_3Ga_3$.

For what concerns the capture mechanism of a I_2 dimer, the relative formation energies $\Omega_{rel}^{(2)}$ compared to those ones of the reactions giving the same final products (i.e., for instance, comparing $\Omega_{rel}^{(2)}$ to $\Omega_{rel}^{(1)}$ for the I_4 reaction product) show that the mechanism, even if exothermic in all the cases studied, seem unlikely to happen except for the case of As_3Ga_2 that is related to the low energetic stability of the reactants As_2 and As_1Ga_2 with respect the As_3Ga_2 cluster.

The above data seem to support the idea of the single interstitial capture process as the main mechanism by which interstitial clusters grow in GaAs, except for the important case of I_6. However a careful analysis of the reaction data of Table II reveals that the growth kinetics of I_n is definitely more complicated and proceeds with almost equal probability through reactions involving single interstitials and di-interstitials. This emerges in a clear way if the reaction-energy data are compared among the competing reactions that share one reactant specie rather than among those reaction that result in the same reaction product. The idea is that as the growing process goes on (n increases) the reaction products can be used as reactants together with lower n reaction products. This view immediately comes out by drawing a flow graph whose nodes are the reaction products and the reactants while the directed edges are labelled with the related reaction energies. Thus, in the beginning of the growth process the only reactant specie is I_1 that can react to produce I_2 through the reaction $I_1+I_1 \rightleftharpoons I_2$. Then, due to the fact that only one part of the isolated interstitials have reacted, I_2 can react with both I_1 and I_2 to produce, respectively, I_3 and I_4, and therefore two directed edges emerge from the I_2 node and heads for the I_3 and I_4 nodes labelled with the relevant reaction energies. Therefore these two reactions compete and the formation of either I_3 or I_4 depends on the relevant reaction energies. The reported data show that the reaction $I_1+I_2 \rightleftharpoons I_3$ is by far favoured against $I_2+I_2 \rightleftharpoons I_4$ (−1.38 eV against −0.6 eV) and thus the growth

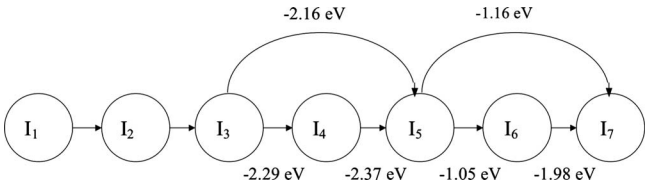

FIG. 11. Schematic flow graph showing how the I_n growth kinetics proceeds. The nodes are the reaction products and the directed edges are labelled with the relevant reaction energy. Refer to Sec. III B for a detailed discussion on the processes involved.

process proceeds again via single interstitial aggregation. Once I_3 are formed, they can react between themselves ($I_3+I_3 \rightleftharpoons I_6$), with I_2 ($I_3+I_2 \rightleftharpoons I_5$) or with I_1 ($I_3+I_1 \rightleftharpoons I_4$). All of these three reaction show remarkable reaction-energy values (−2.15, −2.16, and −2.29 eV, respectively) indicating that I_3 concentration is quite low due to the existence of several low-reaction energy paths involving I_3 as reactant. However in equilibrium the reaction constant is proportional to the product of the reactant concentrations and thus, the reaction $I_3+I_3 \rightleftharpoons I_6$ is practically inhibited being quadratic in $[I_3]$. Therefore the growth process proceeds via I_4 or I_5 with practically the same probability. If the growth process proceeds via I_4 then I_4 could react with I_1, I_2, or I_3 but only the first reaction, i.e., $I_1+I_4 \rightleftharpoons I_5$, takes place because the others have a much lower absolute value of the reaction energy; if the growth proceeds along the other path then I_5 could react with I_1 or I_2 (the reaction with I_3 is excluded in the present analysis because we stopped at $n=7$) with almost the same reaction energy and thus almost the same probability. If this analysis is iterated up to $n=7$, the reaction flow graph shown in Fig. 11 is obtained showing that the growth process proceeds via single interstitial aggregation until $n=3$; for larger n values, the growth process proceeds via four possible reaction paths involving both I_2 and single self-interstitials; in particular, the growth via I_2 coalescence proceeds through odd interstitial clusters, i.e., following the possible sequence $I_3 \Rightarrow I_5 \Rightarrow I_7$.

In Sec. II the reader was reminded that it is a common practice in cluster physics to measure the cluster stability by means of the second-order difference $\Delta_2 E$. Even though the present context is quite different because, as already explained, this quantity is related to the reaction energies differences in a more complicated way, its calculation is still meaningful; indeed, the correction that must be applied to the reaction energy difference (see Sec. II) simply enhances the curve behavior due to the fact that all the As interstitial capture processes have larger reaction energy than the Ga capture processes. Moreover, a better stability evaluation requires the coalescence reaction to be considered that also would enhance the curve behavior. Therefore the second-order differences represents better the true incoming and outcoming reaction flux that is related to the concept of stability.

In Fig. 10(c) the second difference is reported versus n with $2 \leq n \leq 6$ showing that the I_3 complex is the less stable among the investigated I_n complexes while I_5 is a sort of magic cluster, whose stability is markedly higher than the others. The stability curve also shows that I_2 is quite stable thus supporting the idea of I_n cluster growing via either I_1 or I_2 capture process. Thus in ion-implanted GaAs, the formation of As_1Ga_1 and As_3Ga_2 is highly enhanced either through a capture mechanism involving single self-interstitials diffusing in the crystal (for both the I_2 and I_5 clusters) or through the interaction of extend defects (only for the I_5).

C. Electronic properties

The electronic structure of the stable I_n configurations has been studied mainly focusing on the one-electron density of states in the band-gap region (and close to it) and on the localization properties of the one-electron states that are induced by the various defects in the GaAs band gap. In Fig. 10(d) it is reported the number of one-electron levels in the gap (both occupied and empty) versus n where, for convenience, also the case of $n \leq 3$ has been included.

The one-electron density of states in the band-gap region for all the stable I_n configurations are plotted in Fig. 13 while the localization maps of the electrons in the band-gap states are drawn in Figs. 3(c), 5(c), 7(c), and 9(c)–9(f) for the cases of As_2Ga_2, As_3Ga_2, As_3Ga_3, and As_3Ga_4, respectively; the dark gray halos indicate the atoms where more than 10% of the overall gap states are localized.

The Mulliken population analysis has been used to calculate the electronic charge of the atoms involved in the I_n complex and the ones of the surrounding crystal lattice. Keeping in mind that in the bulk phase GaAs exhibits an anion-cation charge transfer of about 0.12 electrons, the charge-transfer maps of the different stable I_n configurations with respect to the bulk have been built and are drawn in Figs. 3(b), 5(b), 7(b), and 9(b)–9(e) for As_2Ga_2, As_3Ga_2, As_3Ga_3, and As_3Ga_4, respectively. Atoms with black halos undergo a loss of electrons (positive charge transfer) with respect the bulk phase while atoms with gray halos experience a gain in electrons (negative charge transfer).

In Fig. 1 are also reported for completeness the charge transfer and the gap states localization maps for stable I_n complexes with $n \leq 3$. The I_4 complex has four levels in the gap at about 0.011, 0.35, 0.77, and 1.20 eV above the valence-band maximum (VBM), and only the first three are occupied by paired electrons. The localization of the one-electron wave functions of the occupied levels in the band gap evidences that these levels, which act as traps for carriers, are strongly localized on the atomic core of the complex. Moreover, all the atoms included in the "core" of the stable As_2Ga_2 complex, except one, undergo a negative charge transfer while a positive charge locates mainly on the atoms of the surrounding lattice.

It should be noted, with respect to the stable As_3Ga_2 complex, that, even if the two quasi-isosceles triangles of the I_5 cluster show similar geometrical features, their electronic properties are quite different. The charge transfer and the wave-function localization [see Figs. 5(b) and 5(c)] show some important differences between the two triangles: the one containing the As atom of the host crystal, for example, has no charge transfer with respect to the bulk case; on the contrary, each atom of the triangle at the Ga site exhibits a significant charge rearrangement of both positive and negative charges. Moreover the band-gap states are spread over

the atoms of the complex and their neighbours, in striking contrast with the I_4 case, and has a quasimirror symmetry. There are four levels in the band gap, at 0.29, 0.59, 1.09, and 1.48 eV above the VBM, the first two of them being doubly occupied while the third is occupied by an unpaired electron.

Also for the stable As_3Ga_3 complex [see Figs. 7(b) and 7(c)], both the charge transfer and the band-gap-states localization are widespread over a large region around the complex containing up to seven hexagons for the charge transfer in the (110) plane view. However, concerning the charge, the scenario is quite different with respect to the previous case because the original nucleation site of the complex, i.e., the right-lower triangular structure at the As site, undergo a positive charge transfer that practically neutralizes the core of the complex (see below). The gap-states localization map is oriented along the direction of the complex that extends along the $[1\bar{1}1]$ direction. Also in this case there are four levels in the band gap at 0.19, 0.57, 0.90, and 1.17 eV above the VBM, the first three of them being occupied by paired electrons while the fourth is empty.

Finally for As_3Ga_4, there are again four levels in the band gap: three of them, located at 0.17, 0.40, and 0.68 eV, are doubly occupied while the last one, at 1.04 eV above the VBM, is occupied by an unpaired electron. Here both the charge transfer and band-gap states appear to be well localized on the self-interstitial atoms of the clusters and on the first neighbours of the host lattice that extend over about eight hexagons in the (110) plane view (see Fig. 9). The original nucleation site corresponding to the right-lower triangular structure at an As lattice site has a negative charge as almost usual except for the I_6 case.

The charge-transfer maps above described show that, in general, the cluster atoms tend to attract electron charges at the expense of the atoms of the host lattice, redeploying the gained electrons in the neighboring atoms of the complex. Such a trend is clearly evidenced in Fig. 12, which reports the charge, evaluated as the difference between the number of electrons and protons, encapsulated in a sphere of radius R and centered in the middle point of the Ga-As bond being the first bulk bond broken to build up the first dumbbell; the different radii have been chosen in such a way to include the same (or almost the same in the nonstochiometric cases) number of Ga and As atoms.

Fig. 12 shows that, for all the stable I_n configurations with $n>3$, the electron charge has an absolute maximum evidencing the formation of a charge excess in the region nearby the I_n complex that is neutralized at about 10 Å from the sphere center. As expected, I_1 and I_2 show a much lower charge separation that is neutralized in a restricted volume [see Fig. 12(a)]; however this charge separation is opposite with respect to I_n $(n>3)$ showing a positive charge very close to the complex that rapidly reverses moving away before being neutralized.

It is worth to evidence the anomalous behavior of I_3 that shows a negatively charged nucleous as the one found for I_n with $n>3$ that reverses at about 10 Å from the complex center, before being neutralized in a much larger volume with respect to the other complexes. This behavior is not fully understood and further analyses are in course that seem

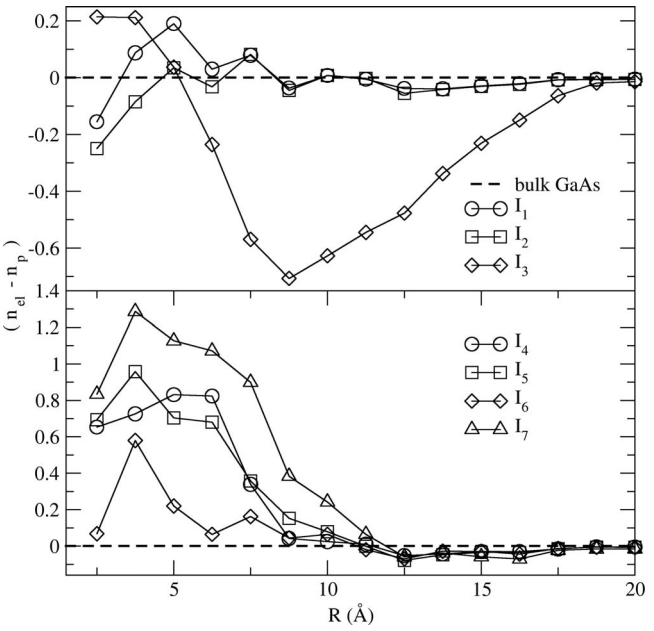

FIG. 12. Fractional charge in the crystal. The number of electrons on atom sites has been computed through the Mulliken population analysis; the curves represent the total charge encapsulated in a sphere centered on the defect inclusions for different radius values (see Sec. III C for details).

to relate it to the particular tetrahedral structure of I_3: this complex basically consists in a tetrahedron that is located at the lattice site formerly occupied by one of the atoms involved; in other words a single lattice atom is replaced by a tetrahedron at the same lattice site. In this way the coordination is in some sense forced not to diverge too much from four so ensuring a "charge continuity" between the complex and the surrounding lattice atoms that could be the reason of such an extended charge exchange. This behavior is inhibited in larger clusters because the tetrahedron is split in triangular structures.

From a simple visual inspection of Fig. 12(b) it arises that, concerning I_n with $n>3$, the I_4 case is slightly different from the others: while I_5, I_6, and I_7 evidence a quite sharp maximum indicating an almost abrupt discontinuity of the charge density, the I_4 charge distribution curve changes much more slowly and show a maximum at larger distance.

To evidence the different features, we calculated the radial charge-density curves from the fitted curves of the I_n charge distributions $(n\geq 4)$ with the hypothesis that the charge density is uniform and different from zero only within a certain spherical sector of radius R; we obtained that, for I_5, I_6, and I_7, the radial charge density changes almost abruptly from negative to positive values at about 3.2 Å from the complex center meaning that the negative/positive-charged regions are quite well separated; the I_4 radial charge density, instead, is a slow varying function of the distance from the complex center that nullifies at 5 Å from the complex center. Notice that the I_6 curve is lower mainly because of different charge transfer and electron localization properties with respect to the other configurations of the atoms forming the triangular structure at the As site [see Fig. 7(b)].

Of course, being the measured charge distribution not uniform in the considered spherical sector, the above radial

charge-density values are affected by large errors that, however, do not compromise the qualitative tendency found showing a better charge separation for I_5, I_6, and I_7. Therefore a wide electrostatic field, with larger intensity for better charge separation, is expected to induce an electrostatic capture volume that can markedly affect the diffusivity of migrating species, such as I_1 and I_2, thus favouring the aggregation process of neutral and positively charged monointerstitial atoms migrating through the crystal, thus favouring the capture and aggregation processes taking place through low-energy reactions. Due to the fact that the charge distribution has no spherical symmetry, the far field is related to the overall dipole moment arising from the complex and the deformed crystal lattice. For As_2Ga_2 and As_2Ga_3 it comes out that the complex related dipole moment is basically oriented along the [110] direction with an additive component along the [100] direction for As_2Ga_3 only. Starting from $n=6$, the dipole moment has a large component oriented along the $[\bar{1}11]$ direction, about 70° away from the $[1\bar{1}1]$ direction of the complex, consistently with the {111} "fingerprint" of such complexes.

In Fig. 10 the HOMO-LUMO energy gaps for the various stable I_n configurations are reported versus n ($1 \leq n \leq 7$) evidencing a minimum for I_3 that thus exhibits a strong metallic behavior in accordance with the previous observation of a large charge-neutralization volume found in this case. As the number n of interstitial atoms increases, the HOMO-LUMO gaps of the stable structures tend to converge to a value between 0.3–0.5 eV; this behavior arises because the number of the one-electron levels in the band gap is a slowly increasing function of the cluster size n, being constant for $4 \leq n \leq 7$ as reported in Fig. 10(c).

Thus, a local semiconductor/semimetal transition arises being related to the HOMO-LUMO energy shrinking for I_n complexes ($4 \leq n \leq 7$); the reason of such a behavior is probably due to a transition between interstitial complexes configurations characterised by a marked configurational symmetry (I_n complexes with small n) to much more complicated defect structures with no local symmetry that deforms the host crystal lattice into a local disordered structure. This results also from the analysis of the electron density of states near the band gap of the bulk phase, reported in Fig. 13 in agreement with the cited increasing number of trap levels in the gap as the size n of the I_n complex increases.

Lastly it is interesting to evidence that for I_n with $n \geq 2$ the 0 K Fermi level pins at 1.0–1.1 eV for all the studied complexes except for I_3 that shows a metallic behavior at the Γ point. The Fermi-level pinning phenomenon is more pronounced for even n complexes being practically fixed at 1.005 eV.

D. Elastic properties

As the size of self-interstitial clusters in the host crystal grows, the local strain field induced by such inclusions affects and modifies the elastic properties of the material. In the frame of the periodic boundary conditions approach, the supercell volume is kept fixed and thus the supercell undergo a compressive deformation that must be related to the actual

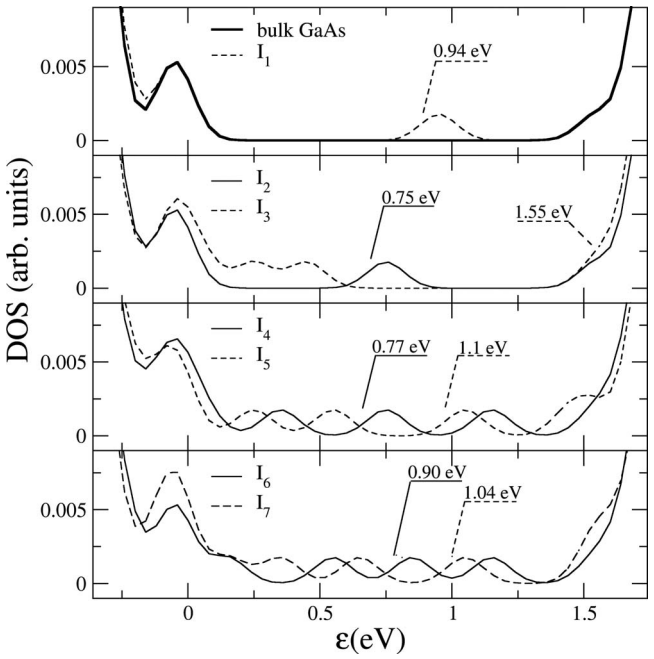

FIG. 13. Electronic density of states near the band gap of bulk GaAs, for I_n with $1 \leq n \leq 7$ complexes. The HOMO levels are reported for all the configurations; notice that the HOMO level for inclusions having odd n, is half filled, while for n even it is completely filled, and that, except for the I_3 case, the zero-temperature Fermi level is pinned at ~1 eV for all the I_n configurations with $n \geq 2$.

elastic energy field that would arise in a real sample. The compressive energy in the supercell is evaluated by measuring the relaxation volume, i.e., by minimizing the supercell total energy versus its volume (i.e., versus the supercell lattice constant) to obtain zero internal pressure via the thermodynamic relation $P=-\frac{\partial E}{\partial V}$; in this condition, the equilibrium atomic volume per atom can be measured.[7] Thus a good test for the minimization procedure described in Sec. II, employed for computing the local strain-field tensor $\epsilon_{\mu\nu}$ at different crystal sites, is to compare the total volumetric deformation induced by the local strain field to the relaxation volume evaluated with the above mentioned standard method. The validation test is reported in the inset of Fig. 14 that shows a good agreement between the relaxation volumes calculated with the two methods; this result strongly supports the reliability of the adopted theoretical framework for the atomistic calculation of the local strain field in the host crystal lattice. Fig. 14 shows that the total volume deformation due to the local strain field increases almost linearly with the size of the self-interstitial cluster. The increasing total relative relaxation volume is, however, less than the one obtained by adding the I_n self-interstitial cluster at the surface of the supercell in bulk phase crystal sites (dotted line).

As a general trend, atoms close to the inclusions tend to experience a tensile stress while next-neighboring shells undergo a compressive strain with an overall expansion of the supercell, as evidenced also from the relaxation volume calculations reported in Fig. 7. The compressive deformation affecting the outer shells of the strain volumes demonstrates how the local strain fields, induced by the nucleation of small

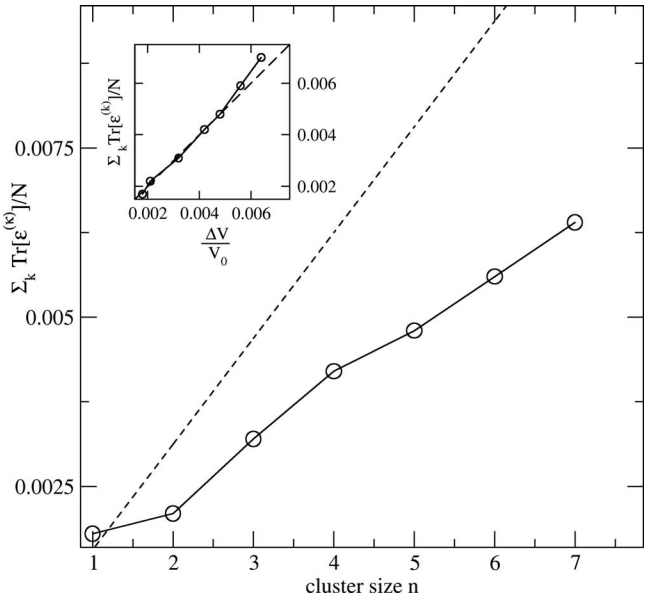

FIG. 14. I_n relative relaxation volume versus the cluster size for $1 \leq n \leq 7$, inside the crystal (solid line) and at the surface (dotted line). In the inset the volumetric strain, computed through the minimization of Eq. (5) is compared to the total volumetric strain computed as function of the relative relaxation volume evaluated via standard techniques (see Sec. III A for more details).

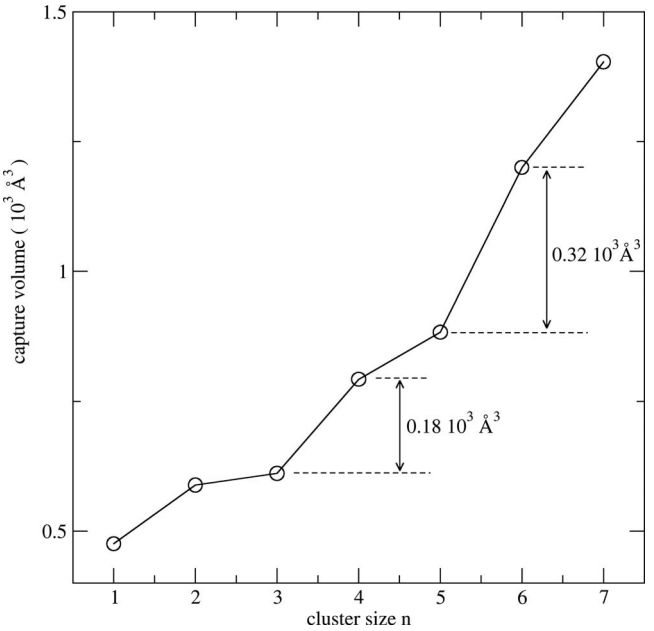

FIG. 15. Capture volume for a diffusing species of the stable I_n with $1 \leq n \leq 7$ configurations as a function of the cluster size.

I_n complexes, could enhance the growth process by driving the migration of mobile self-interstitials and di-interstitials towards the nucleation site in the surrounding region: indeed, diffusing reactive species (see Sec. III B) in the region of compressive strain field close to the core of the I_n complex, tend to be driven by the local negative stress field and relax around the core so favouring the capture process by the nucleation site.

For the configurations studied, it has been evaluated also the capture volume that is defined as the volume of the region containing those lattice atoms whose absolute volumetric change ($\sim \mathrm{Tr}[\epsilon^{(k)}]$) is larger than a given threshold. The results obtained are presented in Fig. 15 where three almost linear regions can be tentatively recognized. As previously mentioned, up to $n=3$ stable I_n configurations are compact structures, basically sharing one lattice site; therefore, as one interstitial is added to a pre-existing single or di-interstitial, the strain field structure and symmetry is certainly changed but the capture volume not so much because the added interstitial is arranged in a site close to the centre of the pre-existing strain field that, consequently, can not extend further too much. Therefore the equilibrium lattice structure of the surrounding region is not affected dramatically by the inclusion for $n \leq 3$. It is worth noticing that the elastic strain field extends freely in any possible direction that is consistent with the symmetry properties of the complex.

For $n \geq 4$ instead, the cluster interacts with many neighboring shells, motivating the choice of expanding the size of the supercell simulation box from 512 atoms, employed in previous works,[13] up to 640 atoms. This is clearly shown in Fig. 15 where the capture volume-change rate undergo a transition between $n=3$ and $n=4$ that corresponds to the situations of a self-interstitial complex affecting only one of two lattice atoms, respectively; indeed, the observed capture volume increase (roughly 0.18×10^3 Å^3) is due to the fact that the fourth interstitial added to I_3 moves an atom away from its original lattice site so that I_4 involves two lattice atoms in the core. The elastic strain introduced by the extra atoms is partially relaxed in the pre-existing I_3 complex that undergo a structural transition from the original tetrahedral structure to a first nucleus of triangular structured network; the remaining elastic energy introduced is relaxed in the surrounding region thus increasing the capture volume. It is interesting to note that from $n=4$ the complex starts to be faceted in the (110) and $(10\bar{1})$ planes.

A second transition is located between $n=5$ and $n=6$ with a volume increase of $\sim 0.32 \times 10^3$ Å^3, which reflects the fact that the complex now involves three lattice atoms. In this case, indeed, the addition of the sixth interstitial to the equilibrium configuration of As_3Ga_2 does not affect too much the pre-existing structure; this means that the elastic energy introduced relaxes very little in the core of the pre-existing complex that, therefore, behaves as a rigid nucleus being already saturated by interstitial and lattice atoms. Thus a large part of the elastic energy must relax into the surrounding lattice by moving an extra lattice atom from its original site to form a "dumbbell" structure quite well separated from the pre-existing complex. This scenario is confirmed also for the As_4Ga_3 case where the seventh interstitial affects very little the I_5 rigid core; the elastic energy introduced relaxes entirely in the surrounding lattice and a I_2-like triangular structure is formed from the pre-existing dumbbell in such a way that the complex can be quite well interpreted as a superposition of I_5 and I_2 structures. A possible scenario for the growth process of I_n for $n \geq 8$ could presumably trace the observed behavior thus involving the formation of ulterior I_5 "rigid cores" along the $[1\bar{1}1]$; the related capture volume increasing rate should most probably saturate.

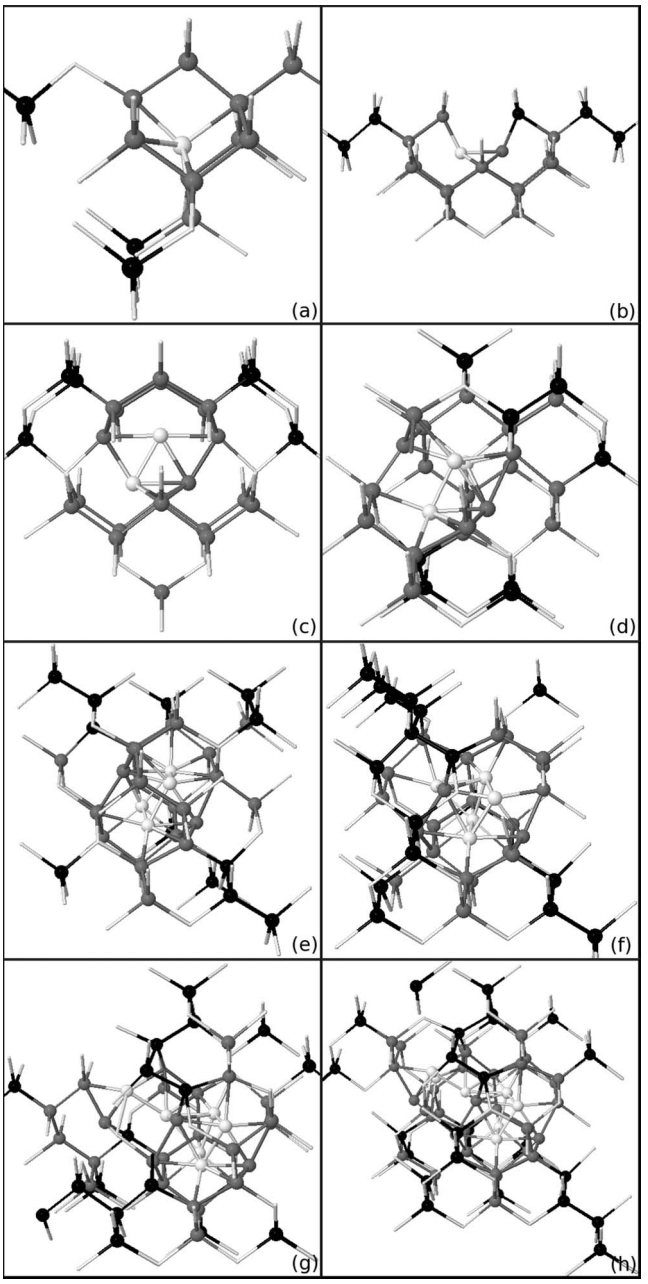

FIG. 16. Local strain fields of the most stable I_n with $1 \leq n \leq 7$ configurations. Atoms under tensile (positive) volumetric strain are marked with gray while black has been used to indicate atoms under compressive (negative) strain; self-interstitial atoms forming the cluster in the host crystal are in white.

Finally Fig. 16 shows the local strain field for all the stable self-interstitials inclusions. The strain fields of I_1 and I_2, reported in Figs. 16(a) and 16(b), respectively, exhibit the same local C_{2v} symmetry of the cluster defects, while the other cases show no particular local symmetries but a clear predominance of strain field patterns along the {111} direction set.

As already mentioned in previous works,[13] the local strain field produced in the host crystal is confined in space for triangular structures, and from Fig. 7(b) it is clear that in this case, the strain field has an approximate spherical symmetry centered on the triangular defect with a capture radius $r_c = (\frac{3V_c}{4\pi})^{1/3} \sim 11.28$ Å. This is probably the reason why extended self-interstitial clusters in GaAs are formed by such structures packed together.

IV. CONCLUSIONS

The properties of ground-state interstitial complex structures I_n (with $n \leq 7$) have been studied by means of semiempirical tight-binding molecular dynamics via an optimization procedure made of a simulated annealing up to a target temperature and a damped dynamics. Due to the complexity of the possible topology, reaction paths and stoichiometry, the analysis has been restricted to I_n with $n \leq 7$ that, anyway, has been shown to be sufficient to extrapolate some important conclusions concerning the growth process of extended defects in GaAs.

The properties of the ground-state structures have been carefully investigated by means of standard methods, such as the Mulliken population analysis, the one-electron wavefunction localization, the atomistic strain-tensor calculation, the binding and the reaction-energy calculations, and the localization of the one-electron states with energy levels in the band gap of the bulk phase.

The general trend emerged from the energetic data show that, in the frame of the adopted approach and in the limits of the used semi-empirical parametrization, I_n complexes have stable configurations against the isolated interstitials and that this is most probably true also for interstitial clusters with $n > 7$. As the complex size increases, the stable configurations found show a marked emerging faceted structure lying in the (110) and $(10\bar{1})$ planes.

Many possible reaction paths have been studied to check for the existence of low energy paths the growth process can proceed through demonstrating that the growth proceeds via either I_1 or I_2 capture by a pre-existing stable complex. In particular, it is interesting to note that the I_2 capture process involves odd n complexes as reactants. The relative importance of I_1 and I_2 capture process could be better clarified if the diffusion activation energy of these two species were known. The I_5 ground-state configuration, namely, the As_3Ga_2 complex, is the most stable I_n complex against the neighbours (I_4 and I_6) as revealed by the second-order difference value that has a maximum in this case. The reaction-energy data, moreover, show that the key units for the I_n growth process are I_1, I_2, and I_5.

The charge analysis have evidenced that atoms forming the defect inclusion tend to attract electron charges at the expense of the atoms of the host lattice redeploying the gained electrons in the neighboring atoms of the complex. Thus, for all the studied complexes with $n \geq 4$, the core undergo a negative charge transfer that is completely neutralized at a distance of about 10 Å from the first nucleation site of the complex. This charge separation is nearly abrupt for all the complexes (except for I_4) indicating the presence of an intense electrostatic field in the surrounding. The far electrostatic field is characterised by a dipole moment that, for "extended defects" (i.e., $n > 5$), has a large component oriented along the $[\bar{1}11]$ direction, i.e., 70° away from the

growth direction of the complex, while the I_5 dipole moment, that must be considered as the building block of linear I_n complexes whose core nucleates along the $[1\bar{1}1]$ direction, has two low-index components.

Localization analysis have pointed out that levels in the band gap are strongly localized at the atoms of the extended defect acting as traps for the charge carriers and thus resulting a net shortening of their lifetime. The Fermi level pins around 1.0–1.1 eV and the electronic structure undergo a local semiconductor-semimetal transition (HOMO-LUMO energy shrinking for the well-localized gap states).

The atomistic calculation of the local strain allowed for the calculation of the relaxation volume that comes out to be quasilinear with the complex size. However, a more careful analysis of the local strain maps revealed the tensile-compressive structure of the strain field induced by I_n that, for $n>5$, is clearly oriented along the $[1\bar{1}1]$ growth direction.

The atomistic local strain-field maps have been employed to estimate the capture volumes for diffusing species (such as I_1 and I_2) into the crystal during ion-implantation or the subsequent annealing stage; the analysis of this quantity for the different stable structures strongly supports the idea that the I_5 ground-state configuration can be considered as a sort of building unit of the rigid core for {111} oriented extended defects in GaAs. The elastic analysis has pointed out the importance of triangular structures as the ones minimizing the strain field induced by a defect cluster on the atoms of the host lattice.

These considerations, together with a detailed energetic analysis above discussed, support the proposal of the As_3Ga_2 complex, made of two triangles on different crystal sites and a single monointerstitial atom, as the nucleation seed for {111}-oriented extended defect complexes in GaAs, such as dislocations or stacking faults.

*Corresponding author; fabrizio.gala@uniroma1.it

[1] T. E. M. Staab, R. M. Nieminen, J. Gebauer, R. Krause-Rehberg, M. Luysberg, M. Haugk, and T. Frauenheim, Phys. Rev. Lett. **87**, 045504 (2001).
[2] I. Ca'mara Mayorga, E. A. Michael, A. Schimtz, P. van der Wal, R. Güsten, K. Maier, and A. Dewald, Appl. Phys. Lett. **91**, 031107 (2007).
[3] H. T. H. Boudinov, A. V. P. Coelho, and C. Jagadish, J. Appl. Phys. **93**, 3234 (2003).
[4] G. Vitali, G. Zollo, C. Pizzuto, M. Rossi, D. Manno, and M. Kalitzova, Appl. Phys. Lett. **69**, 4072 (1996).
[5] G. Zollo, C. Pizzuto, G. Vitali, M. Kalitzova, and D. Manno, J. Appl. Phys. **88**, 1806 (2000).
[6] D. J. Chadi, Phys. Rev. Lett. **41**, 1062 (1978).
[7] J. E. Northrup and S. B. Zhang, Phys. Rev. B **47**, 6791 (1993).
[8] G. Zollo, Y. J. Lee, and R. M. Nieminen, J. Phys.: Condens. Matter **16**, 8991 (2004).
[9] G. Zollo and F. Gala, Phys. Rev. B **77**, 094125 (2008).
[10] M. A. Malouin, F. El-Mellouhi, and N. Mousseau, Phys. Rev. B **76**, 045211 (2007).
[11] G. Zollo and R. Nieminen, J. Phys.: Condens. Matter **15**, 843 (2003).
[12] M. Volpe, G. Zollo, and L. Colombo, Phys. Rev. B **71**, 075207 (2005).
[13] G. Zollo and F. Gala, Phys. Rev. B **75**, 115205 (2007).
[14] L. Colombo, Riv. Nuovo Cimento **28**, 1 (2006).
[15] C. Molteni, L. Colombo, and L. Miglio, J. Phys.: Condens. Matter **6**, 5243 (1994).
[16] H. Seong and L. J. Lewis, Phys. Rev. B **52**, 5675 (1995).
[17] M. P. V. S. Kirkpatrick and C. D. Gelatt, Jr., Science **220**, 671 (1983).
[18] S. B. Zhang and J. E. Northrup, Phys. Rev. Lett. **67**, 2339 (1991).
[19] B. Song, C. H. Yao, and P. L. Cao, Phys. Rev. B **74**, 035306 (2006).
[20] M. L. Falk, Phys. Rev. B **60**, 7062 (1999).
[21] M. Tang, L. Colombo, J. Zhu, and T. Diaz de la Rubia, Phys. Rev. B **55**, 14279 (1997).